Supporting material:
Permeabilized rat cardiomyocyte response demonstrates intracellular origin of diffusion obstacles

Natalja Jepihhina, Nathalie Beraud, Mervi Sepp, Rikke Birkedal, and Marko Vendelin
Laboratory of Systems Biology, Institute of Cybernetics, Tallinn University of Technology, Akadeemia 21, 12618 Tallinn, Estonia

The supporting material includes detailed description of used solutions, mathematical models, and fluorescence spectra recorded in fluorometer.

MATERIALS AND METHODS

Experimental procedures

Solutions used in isolation of cardiomyocytes. Wash solution contained (in mM): 117 NaCl (Sigma-Aldrich, 71379), 5.7 KCl (Sigma-Aldrich, P5405), 4.4 $NaHCO_3$ (Sigma-Aldrich, S6014), 1.5 KH_2PO_4 (Sigma-Aldrich, P0662), 1.7 $MgCl_2$ (Sigma-Aldrich, 63068), 21 HEPES (Sigma-Aldrich, H3375), 20 Taurine (Sigma-Aldrich, 86329), 11.7 Glucose (Sigma-Aldrich, 158968), and pH was adjusted at 25°C to 7.4 with NaOH.

Digestion solution had the same composition as the wash solution with the addition of 3mg/ml BSA (Roche, 10 775 835 001), 0.375 mg/ml collagenase P (Roche). In some cases, 75 μM EGTA was added to the digestion solution due to high amounts of Ca^{2+} in the collagenase.

Sedimentation solution had the same composition as the wash solution with the addition of 2mg/ml BSA (Roche, 10 775 835 001), 10 μM leupeptine (Roche, 11 034 626 001), 2 μM soybean trypsin inhibitor (Fluka, 93619).

Fluorescence microscope. Microscope experiments were performed on an inverted Nikon Eclipse Ti-U microscope (Nikon, Japan) equipped with two tiers of motorized filter turrets for simultaneous acquisition of transmission and fluorescence images. For transmission images, light from the 100W halogen microscope lamp was passed through a 585/40 nm filter onto the specimen and through the dichroic filters in the turrets to a high-speed CCD camera (IPX-VGA210-LMCN, Imprx Inc., Florida, USA) mounted on the left port. For images of NADH and FP autofluorescence, respectively, light from a Prior Lumen 200 with a 200W metal halide lamp with extended wavelength (Prior Scientific, Cambridge, United Kingdom) was passed via an optical fiber into the upper filter turret. For NADH recordings, the light was passed through a 340/26 nm excitation filter onto a 400 nm long pass dichroic mirror, which deflected the light onto the specimen. Light emitted from the specimen passed back through the upper filter cube to a 510 XR dichroic in the lower filter cube and reflected through a 460/80 nm emission filter to an Andor Ixon EMCCD camera (Andor Technologies, Belfast, United Kingdom). For FP recordings, the light was passed through a 465/30 nm excitation filter onto a 510 nm dichroic mirror, which deflected the light onto the specimen. Light emitted from the specimen passed back through the upper filter cube to a 560 XR dichroic in the lower filter cube and reflected through a 525/50 nm emission filter. All filters were purchased from AHF analysentechnik AG, Germany. Transmission images together with images of NADH or FP autofluorescence were acquired every 30 sec. To reduce photobleaching, a Uniblitz shutter (VCM-D1, Vincent Associates, Rochester, USA) timed the light exposure with the acquisition.

Analysis of fluorescence signal. Fluorescence signal intensity from microscope single cell experiments was analyzed using ImageJ software. Both cell containing and background regions were selected and corresponding average fluorescence signal intensities were determined with ImageJ plug-in "measure stack". Then, background fluorescence was subtracted from cell fluorescence and data plotted on a time-scale. From the latter plot, average fluorescence was found for each condition to which the cell was exposed (ADP concentration, uncoupling or block of oxidative phosphorylation).

Data obtained from spectrofluorophotometer experiments was analyzed with home-made software written in Python. We integrated the recorded spectra in the ranges corresponding to the optical filters used in the fluorescence microscope: 420-500 nm and 500-550 nm for NADH and FP autofluorescence, respec-

tively.

Fluorescence signal recorded in microscope or fluorometer was normalized to the signal values in reduced and oxidized states. Mitochondria were reduced by oligomycin and cyanide (OL+CN); oxidized state was recorded either in the beginning of the experiment before addition of substrates in the presence of ADP or by adding FCCP at the end of the experiment. The following equations were used:

$$f_{NADH} = \frac{F - F_{OX}}{F_{RED} - F_{OX}},$$
$$f_{FP} = \frac{F - F_{RED}}{F_{OX} - F_{RED}},$$

where F was recorded fluorescence; F_{OX} and F_{RED} was fluorescence recorded in oxidized or reduced state, respectively.

Solutions. Substrate-free mitomed solution contained (in mM): 3.0 KH_2PO_4 (Sigma-Aldrich, P0662), 3.0 $MgCl_2$ (Sigma-Aldrich, 63068), 20 HEPES (Sigma-Aldrich, H3375), 0.5 EGTA (Sigma-Aldrich, 03778), 20 taurine (Sigma-Aldrich, 86329), 0.5 dithiothreitol (Sigma-Aldrich, D0632) and 60 lactobionate (Sigma-Aldrich, L2398). 5 glutamate (Sigma-Aldrich, 49449) and 2 malate (Sigma-Aldrich, M6413) were added as substrates together with 110 sucrose (Sigma-Aldrich, S1888), pH was adjusted at 25°C to 7.1 with KOH.

Concentrations of the uncoupler and respiration blockers were: FCCP (Carbonyl cyanide 4-(trifluoromethoxy)phenylhydrazone, 10μM, Ascent Scientific, Asc-081), oligomycin A (10μM, Tebubio, 579-13-5), and sodium cyanide (5mM, Sigma-Aldrich, 205222).

Mathematical models

Compartmentalized model of rat cardiomyocyte energetics. The mathematical model of permeabilized rat cardiomyocyte was taken from (1). Among the models analyzed in (1), the models '3s' and '4s' were found to describe respiration and other measurements best. Here, the results obtained with the model '3s' are presented. Calculations with model '4s' led to almost the same results (results not shown). In short, the models consider permeabilized rat cardiomyocytes divided into several compartments: mitochondria, cytosol, and a small compartment inducing functional coupling between endogenous pyruvate kinase and fraction of ATPases. In addition, solution surrounding the cells is considered as well. All compartments are separated from each other by diffusion restrictions including the connection between solution and cytosolic compartment. As a result, concentrations of the metabolites are different in different compartment and could differ from the concentrations in surrounding solution. The concentrations and the rates of reactions are determined by relative activities of the enzymes and extent of diffusion restrictions. Model parameters were taken from (1).

Model of solution flow in microscope chamber and in the vicinity of the cell. To find the flow velocity profile in the fast exchange chamber and in the vicinity of the cell, Navier-Stokes equations for incompressible fluid were solved. Simulations were performed using *icoFoam* solver for laminar, isothermal, incompressible flow of Newtonian fluids from OpenFOAM toolbox (`http://www.openfoam.com`). The kinematic viscosity of fluid was taken equal to 10^{-6} m^2/s.

To find the flux velocity profile in microscope flow chamber, the geometry of the chamber was approximated by a diamond shape with the corners cut at in- and out-flow. The chamber was taken as 6 mm wide and 15 mm long. The openings were 1.33 mm wide for inflow and 2 mm for outflow and located 7 mm and 6 mm, respectively, from the center of the diamond. The chamber was modeled assuming 1 mm deep solution. As a boundary condition, non-flow condition (velocity was zero, normal gradient of pressure was zero) was specified for chamber walls. On the upper surface of solution, the solution was considered to move freely along that surface (*slip* boundary condition: normal gradient of pressure was zero, normal component of velocity was zero, gradient of tangential components of velocity were zero). On inflow, uniform velocity was assumed (0.00625m/s corresponding to 0.5ml/min) with normal gradient of pressure equal to zero. On outflow, pressure was assumed to be 0 Pa and normal gradient of velocity was set to zero.

To find the velocity profile in the vicinity of the cell, simulations were performed in a box with the sides of 600μm along the flow (x-axis), 600 μm wide (y-axis) and 300 μm high (z-axis) that was considered

to be situated in the center of the diamond chamber. The cell (modeled as a box with the sides 100 μm along the flow, 20 μm wide and 20 μm high) was positioned on the bottom of the simulation box and the no-flow conditions were given on the boundary of permeabilized cell (velocity zero, normal gradient of pressure zero). No-flow boundary conditions were applied on the bottom of the simulation box, as corresponding to the cover glass. In accordance with the simulation of the flow in the microscope chamber (see results), the flow surrounding the simulation box was considered to have only one non-zero velocity component (v_x), parallel to x-axis, that depend only on the distance from the glass z: $v_x = az^2 + bz$ (a and b were found by fitting the velocity profile calculated for the middle of a chamber). As a boundary condition, the velocity was given on the entrance into the simulation box and on the top wall (on those walls the normal gradient of pressure set to zero) and calculated assuming no normal gradient on the outflow wall (pressure set to zero). On the walls parallel to the flow, *slip* boundary condition was used.

The finite volume meshes for both cases were generated by using CUBIT tool suite (Sandia National Laboratories, New Mexico, USA, `http://cubit.sandia.gov`) with hexahedral element sizes of 50 μm and 5 μm for chamber and cell surroundings simulations, respectively. As an initial condition, pressure and velocity of the fluid was set to zero. Simulations were performed until solution stabilized (few seconds) with steady-state flow profile used in the further analysis.

Reaction-diffusion-convection model of cell surroundings. To quantify the influence of solution flow around the cell in the microscope chamber on measurements, we composed the mathematical model that took into account mitochondrial oxidative phosphorylation, diffusion of ADP in solution and the cell, and convection of ADP by flow of solution surrounding the cell. For simplicity, only ADP was followed and it was assumed that ADP is consumed by mitochondrial OxPhos only. Similar to bidomain approach in modeling electrophysiology, OxPhos reaction was given in continuum within the cell and reaction rate was described by Michaelis-Menten equation. Apparent Km(ADP) of reaction was changed to reflect the influence of intracellular diffusion obstacles from 0.015 mM (no significant intracellular diffusion obstacles, same affinity as isolated mitochondria) to higher values (increased contribution of intracellular diffusion restrictions). The maximal mitochondrial ATP synthase activity in the cell was taken as 0.54 mM ATP/s, taking into account ADP/O_2 ratio (6), maximal mitochondrial respiration rate (13.5 μmol O_2/min·g ww), wet weight to dry weight ratio (5), and volume to wet weight ratio (0.5 ml/g ww), as in (2). This activity is somewhat higher than 0.41 mM/s used by Kongas et al. (3). Diffusion coefficient of ADP in solution was taken equal to 397 μm^2/s (3) and reduced to 41% of this value in the cell (4).

The simulation box was 450μm along the flow, 300μm wide, and 150μm high. The cell (same dimensions as in flow calculations above) was positioned on the bottom, 140 μm from inflow into the simulation box. The flow velocity calculated by the other models was used to describe convection of ADP. As boundary conditions, no-flow (normal gradient of ADP was zero) was allowed on the bottom of the simulation box (corresponding to cover glass) and the ADP concentration on the other borders was set equal to the concentration used in experimental solution. For comparison, simulations with no convection were also performed. In those simulations, flow rate was set to zero and the simulation box was increased to 600μm $\times$ 600μm $\times$ 300μm.

The finite element model solving partial derivative equation corresponding to reaction-diffusion-convection system was implemented in deal.II package (5). Finite element size was 2.5 μm. Integration was performed until steady-state was reached with the steady state solution used in the analysis to calculate respiration rate of the cell.

RESULTS

Fluorescence spectra recorded in fluorometer. In the first series of experiments (*n*=7), we used the same normalization of fluorescence signal as in the experiments performed in microscope chamber. However, use of FCCP in fluorometer resulted in alteration of recorded spectra that made it impossible to use. Namely, FCCP has a considerable absorbance in a wide range of wavelengths with a maximal absorbance at $\sim$380 nm. As it was evident from

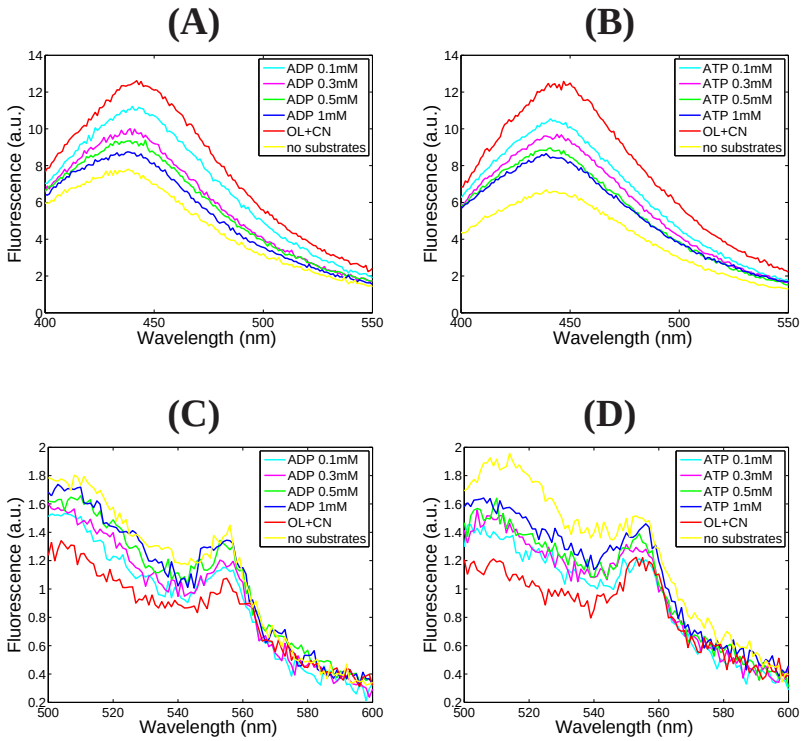

FIG. S1: Fluorescence spectra recorded with excitation light of 340nm (top row) or 465nm (bottom row). Solution with the permeabilized cardiomyocytes was exposed to different levels of exogenous ADP (left column) or ATP (right column) as well as OL+CN. In the beginning of the experiment, spectrum corresponding to oxidized state of mitochondria was recorded in the absence of substrates.

the shape of the NADH fluorescence spectrum when recorded in fluorometer, fluorescence was reduced at wavelengths below 450 nm. For recorded FP fluorescence the influence of FCCP was even larger: FP fluorescence in the presence of FCCP was smaller than fluorescence recorded in the presence of ADP or ATP. Note that this is opposite to expected fluorescence level and the results obtained on a single cell level in microscope. This effect of FCCP in fluorometer and the differences in recorded signal in microscope and fluorometer can be attributed to the optical pathways in those experiments. In the inverted microscope, the cells are recorded while sedimented to the cover glass. As a result, the microscope camera records the signal that comes from the cell, and passes the cover glass and microscope optics (objective, dichroic mirror, emission filter and tube lens). In the fluorometer, cells are in suspension and before excitation light can reach the cell it has to pass the solution. The same applies to the emitted light. While not a problem when cells are exposed to solution with low absorbance, the difference in optical pathways becomes important in solutions that have significant absorbance, as after addition of FCCP.

To avoid the influence of FCCP in the fluorometer recordings, we used for normalization the fluorescence of permeabilized cells recorded in the absence of substrates (but in the presence of low ADP or ATP). Due to the absence of substrates, mitochondria were in oxidized state leading to high FP and low NADH fluorescence. After recording of the spectra without substrates, spectra were recorded in the presence of different concentrations of ADP or ATP and, in the end of the experiment, in the presence of OL+CN. Representative spectra are shown in Fig. S1.

SUPPORTING REFERENCES

1. Sepp, M., M. Vendelin, H. Vija, and R. Birkedal, 2010. ADP compartmentation analysis reveals coupling between pyruvate kinase and ATPases in heart muscle. *Biophys J* 98:2785–2793.

2. Vendelin, M., M. Eimre, E. Seppet, N. Peet, T. Andrienko, M. Lemba, J. Engelbrecht, E. K. Seppet, and V. A. Saks, 2004. Intracellular diffusion of adenosine phosphates is locally restricted in cardiac muscle. *Mol Cell Biochem* 256-257:229–241.
3. Kongas, O., T. L. Yuen, M. J. Wagner, J. H. G. M. V. Beek, and K. Krab, 2002. High K(m) of oxidative phosphorylation for ADP in skinned muscle fibers: where does it stem from? *Am J Physiol Cell Physiol* 283:C743–C751.
4. Kushmerick, M. J., and R. J. Podolsky, 1969. Ionic mobility in muscle cells. *Science* 166:1297–1298.
5. Bangerth, W., R. Hartmann, and G. Kanschat, 2007. deal.II — a General Purpose Object Oriented Finite Element Library. *ACM Transactions on Mathematical Software* 33:24.